Airfoil Table Generation Comparison Utilizing XFOIL and UNS2D Flow Solvers

Gianmarco Sahragard-Monfared
Aerospace Engineer
NASA Ames Research Center
Aeromechanics Office
Moffett Field, CA, USA

Isaac Cavazos
Student
California State University, Sacramento
Dept. of Mechanical Engineering
Sacramento, CA, USA

Joseph Gabriel Estrada
Student
California State University, Sacramento
Dept. of Mechanical Engineering
Sacramento, CA, USA

Dalton Hall
Student
California State University, Sacramento
Dept. of Mechanical Engineering
Sacramento, CA, USA

Sarah Maadarani
Student
California State University, Sacramento
Dept. of Mechanical Engineering
Sacramento, CA, USA

Min Kaung Myat
Student
California State University, Sacramento
Dept. of Mechanical Engineering
Sacramento, CA, USA

ABSTRACT

The flow solvers XFOIL and UNS2D were utilized within the airfoil table generator AFTGen to generate airfoil performance tables, and these results were compared to determine accuracy at low Mach numbers that may be relevant to Urban Air Mobiltiy (UAM) applications. Airfoil tables were generated for the NACA 0012 airfoil as well as a set of three asymmetrical airfoils developed in this study from which the rotor blade CSUS 001 was comprised. To determine which solver more accurately represented real-world aerodynamics, the airfoils were experimentally tested in the CSU 2-foot by 2-foot wind tunnel. The results of XFOIL and UNS2D were compared to the experimental results. It is important to note that due to differences in the Reynolds numbers between simulations and experimental testing, the magnitude of the section lift and drag coefficient varies between the two methods. However, observations on the accuracy of XFOIL and UNS2D could still be made based on the trends of the data. For the symmetrical NACA 0012 airfoil, it was found that XFOIL and UNS2D accurately predicted the trends of the section lift and drag coefficients. However, XFOIL predicted slightly lower section drag coefficients than UNS2D for the tested angles of attack. For the asymmetrical CSUS 001 airfoils, XFOIL could not predict a steady to decreasing section lift coefficient phenomenon at negative angles of attack observed in both the UNS2D and experimental results. Similarly, XFOIL was unable to predict an increased section drag coefficient at negative angles of attack for the CSUS 001 airfoils as observed in the UNS2D and experimental results. Additionally, 3D computational fluid dynamics was utilized through RotCFD to compare the performance of a rotor blade using the CSUS 001 airfoils versus a rotor blade using the NACA 0012 airfoil.

NOTATION

A	surface area of rotor
α	angle of attack, degrees
C	airfoil chord length
c_d	section drag coefficient, $c_d = (2F_D)/(\rho v^2 A)$
c_l	section lift coefficient, $c_l = (2F_L)/(\rho v^2 A)$
c_m	section moment coefficient, $c_m = (2F_M)/(\rho v^2 Al)$
C_P	power coefficient
C_T	thrust coefficient
C_T/σ_s	blade loading, $C_T/\sigma_s = C_T/(N_B * c/(2\pi R))$
CFD	computational fluid dynamics
$Deg.$	collective angle
F_D	drag force, Newtons, $F_D = c_d * \rho(v^2/2)A$
F_L	lift force, Newtons, $F_L = c_l * \rho(v^2/2)A$
F_M	moment force, Newtons, $F_M = c_m * \rho(v^2/2)Al$
FM	figure of merit, $FM = C_T^{(3/2)}\sqrt{2})/C_P$
H	shape parameter at the end of wake
l	reference length, meters
M	Mach number
m	maximum camber
M_{Tip}	tip Mach number
N_B	number of blades
P	pressure, pascals
p	location of maximum camber
q	total pressure (Bernoulli)
r	radial station of specified airfoil
R	overall radius of entire blade
Re	Reynolds number, $Re = \rho v l/\mu$
ρ	fluid density around airfoil, kilograms per cubic meter
σ_s	solidity of the blade, dimensionless, $\sigma_s = (N_B * c)/(\pi R)$
T	temperature, Kelvin

t	maximum thickness, percent of chord
θ	momentum thickness at end of wake
θ_i	momentum thickness downstream
u	edge velocity at end of wake, meters per second
v	fluid velocity around airfoil, meters per second
V	freestream velocity, meters per second

INTRODUCTION

Urban Air Mobility (UAM) efforts are currently driving research initiatives aimed at enhancing the accessibility of current air vehicles, such as helicopters, for public use and emergency response systems. Rotor blade design is a critical aspect of rotorcraft performance, with the geometric aspects influencing flight characteristics. The lift-to-drag ratio is the balance of two forces correlated to the blade's total lift force and drag force. By maximizing the lift-to-drag ratio, it is possible to increase the efficiency of rotorcraft and make them more practical for urban air mobility. This can be achieved by utilizing software that mimics real-life conditions under which the rotorcraft will perform.

A similar study to the one presented in this work was performed by Kallstrom (Ref. 1) utilizing AFTGen (Ref. 2) to compare the flow solvers XFOIL (Ref. 3) and OVERFLOW (Ref. 4). Kallstrom observed that XFOIL is limited in angle of attack range and thus cannot accurately model stall and post-stall conditions. Kallstrom also stated that OVERFLOW does not perform well at low Mach numbers, with the best performance occurring at Mach numbers of 0.4 and above. However, it is important to acknowledge that AFTGen limits the capability of higher fidelity flow solvers such as OVERFLOW. Additionally, Kallstrom noted that the solving time of XFOIL is much faster than OVERFLOW. Therefore, this study investigates if UNS2D (Ref. 5 and 6), a flow solver made specifically for use with AFTGen, performs better than XFOIL at low Mach numbers. This study utilizes an NACA 0012 airfoil as well as custom asymmetric airfoils (used to generate the CSUS 001 rotor blade) to compare XFOIL and UNS2D. The success of each airfoil generation tool was determined by comparing its predictions with experimental data acquired through wind tunnel testing. Additionally, the aerodynamic performance of CSUS 001 was compared to a rotor blade generated from the NACA 0012 airfoil utilizing the computational fluid dynamics (CFD) tool RotCFD.

In the design process, CFD simulations are utilized to anticipate and reduce uncertain factors such as fluid behavior around the blade, rotor performance, and boundary condition influences. This enables the most cost-effective evaluation of design iterations as needed and helps shape future changes to achieve the desired blade performance characteristics.

For this study, a list of functions and specifications were created in tandem with the goal of creating an optimized blade design: a novel blade geometry is developed; the blade radius must fit within a 2-foot by 2-foot wind tunnel; the blade design must deliver a 30:1 lift-to-drag ratio; and the rotors should achieve higher figure of merit, in the tested collective range, than NACA 0012 blades.

One of the primary ways to manipulate an airfoil profile for an effective design that produces a favorable lift-to-drag ratio is to align the airfoil profile to that of a symmetrical or asymmetrical airfoil shape. The symmetrical airfoil profile produces no lift at an angle of attack of zero, is heavy and stable, and has no camber due to the identical lower and upper surfaces. The asymmetrical airfoil creates a good lift-to-drag ratio even at low angles of attack and produces a lift force when oriented at an angle of attack of zero due to its camber.

A study by Thakur and Choudhary (Ref. 7) compares the characteristics of an asymmetrical airfoil profile with the symmetrical airfoil profile of the NACA 0012. At an angle of attack of zero, it was determined that the symmetrical airfoil had a lower section lift coefficient compared to the asymmetrical airfoil due to its camber (Ref. 7).

APPROACH

An asymmetrical blade was utilized due to the increased lift-to-drag ratio at low angles of attack compared to a symmetrical airfoil. Then a viable airfoil shape with that characteristic was created and validated with the 2D flow solvers XFOIL and UNS2D within AFTGen. After verifying that the blade geometry and performance had successfully converged at various angles of attack and Mach number, the next step was the utilization of the 3D solver to test the blades in an isolated rotor hover configuration within RotCFD. This allowed for efficiency assessment by looking at factors such as power coefficient, C_P, and thrust coefficient, C_T. Once computational analyses and simulations were complete, physical testing in a wind tunnel was performed to validate the aerodynamic coefficients and rotor performance data obtained from the 2D and 3D simulations.

Furthermore, to ensure the consistency of this process, testing of the NACA 4-series airfoil and the custom designed CSUS 001 airfoil were done concurrently. The NACA 0012 airfoil was chosen due to the large amount of public domain experimental data available for comparison.

The wind tunnel wind speed and size limitations restricted the tested Reynolds number to 1.39×10^5 at a Mach number of 0.1. Due to a current inability of the flow solvers to converge at low Reynolds numbers, an Re/M of 3.24×10^6 was used for UNS2D and XFOIL analysis. Despite the two order of magnitude difference in Reynolds number between experimental testing and flow solver analysis, observations could still be made based on data trends.

DESIGN

Airfoil shape

Developing an airfoil design involves using simulations to understand the physical principles and aerodynamic characteristics of an asymmetrical airfoil profile and

consideration of the aspects of basic airfoil behaviors such as generating aerodynamic lift, drag, and pressure variance at different angles of attack. As part of the design modification process, exploring airfoil databases such as the NACA 4-digit series asymmetrical airfoil shape is essential in obtaining the desired airfoil applications. In the final CSUS 001 blade design, three airfoils with various thicknesses such as 11%, 13%, and 15% thickness-to-chord ratio with a camber of 9% were placed at three radial stations along the span of the blade, as detailed in Table 1.

Table 1: CSUS 001 Airfoil Specifications at Various Radial Stations

Airfoil	Thickness	Camber	Chord Length (inches)	Radial Station (r/R)
Airfoil 1	15%	9%	2.5	0.445
Airfoil 2	13%	9%	2.5	0.771
Airfoil 3	11%	9%	2.5	1.0

MATLAB code

MATLAB was utilized to generate the geometry of the custom airfoil. The NACA series four airfoil equations were modified and used as the basis for the airfoil. The MATLAB script allowed the user to specify the maximum thickness of the airfoil, the location of maximum thickness, the camber of the airfoil, the location of maximum camber, as well as the number of points to be generated. From these inputs MATLAB plotted the airfoil and wrote the X and Y coordinates into a text file that could then be used as input for airfoil table generators within AFTGen. The equation used to generate the uncambered upper surface of the airfoils is shown in Equation 1.

$$y = 5t \left(.51x^{1/2} - .3291x - .1562x^2 + .0789x^3 - 0.1015x^4\right) \quad (1)$$

Where t is the maximum thickness as a percentage of the chord. The uncambered bottom surface of the airfoil was created using Equation 2.

$$y = 5t \left(.61x^{1/2} - .6291x - .1562x^2 + .3789x^3 - 0.2020x^4\right) \quad (2)$$

Where t is the same value as in the top surface equation. The value x is then calculated between zero and one on an equally spaced vector with as many points as specified by the user. After the uncambered airfoil shape has been generated and plotted, the code then applies the cambering equation, Equations 3 and 4, to both the top and bottom surfaces. This equation is identical to that used in the NACA series 4 airfoils.

$$y = \frac{m}{p}(2px - x^2) \; 0 \leq x \leq p \quad (3)$$

$$y = \frac{m}{(1-p^2)}\left((1 - 2p) + 2px - x^2\right) p \leq x \leq 1 \quad (4)$$

Where m is the maximum camber and p is the location of maximum   camber.

Changes

The earliest concept of the blade design originally consisted of five distinct airfoils starting at 13% thickness-to-chord ratio near the hub and decreasing until it reached 5% thickness-to-chord ratio at the end of the blade. This design had the same camber of 9% throughout all design with airfoils placed at five radial stations along the blade. However, as previously stated, the number of airfoils decreased to three. This was a result of the airfoil generation within the CFD solvers provided and the realization that an airfoil with a thickness of 5% would be difficult to print for physical testing. Figure 1 illustrates the final design of the CSUS 001 rotor blade.
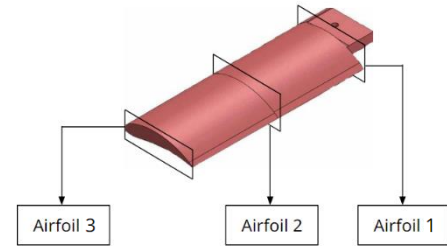

Figure 1: CSUS 001 Rotor Blade

COMPUTATIONAL METHODS

As stated previously in the approach section, 2D and 3D solvers were utilized to determine the aerodynamic properties of the airfoils being tested and generated using AFTGen between the angles of attack of -10 and 10 degrees and Mach numbers ranging from 0.1 to 0.3. Developed by Sukra-Helitek, AFTGen provides a GUI for various flow solvers, including XFOIL, ARC2D, OVERFLOW, UNS2D, MSES, and UNS2D (Ref. 2).

The 3D software RotCFD was used to "test" the three airfoils used in the CSUS 001 rotor blade, and the NACA 0012 airfoil to determine their efficiency when loaded on a rotor blade within a rotorcraft configuration. The simulation setup was appropriately adjusted to obtain converged results for the coefficient of thrust (CT) and total coefficient of power (CP). Detailed information on the input settings for RotCFD and rotor specifications can be found in the RotCFD Testing section.

XFOIL

XFOIL is an airfoil analysis program developed by Prof. Mark Drela at MIT, and it is able to quickly analyze inviscid and viscous flows around a 2D airfoil for subsonic flight conditions. The XFOIL solver utilizes an integral-based approach to determine the section lift coefficient (c_l), section drag coefficient (c_d), and section moment coefficient (c_m) of the blade. This integral considers the values from both ends of the panel being assessed and iteratively calculates the aerodynamic coefficients until convergence (Ref. 3).

3

To obtain converged values for the airfoil aerodynamic coefficients, the solver first finds the pressure distribution over the panels or surface of the airfoil, which utilizes the user-inputs for the flow conditions provided. Subsequently, this allows the solver to solve for the velocity and allows for the integral approach of the pressure along the airfoil's surface to calculate the airfoil's aerodynamic properties. The integral approximation approach can be described by utilizing Equations 5, 6, 7, and 8 (Ref. 3).

$$c_l = \frac{L}{q} = \int c_p d\underline{x} \qquad (5)$$

$$c_m = \frac{M}{q} = \int -c_p[(x - xref)dx + (y - yref)dy] \qquad (6)$$

$$c_d = \frac{D}{q} = \int 2\theta_i = 2\theta\left(\frac{u}{V}\right)^{\frac{H+5}{2}} \qquad (7)$$

$$q = 0.5 * r * V^2 \qquad (8)$$

Where q is the total pressure (assuming that there is no static pressure), θ is the momentum thickness at the end of the wake, u is the edge velocity at the end of the wake, H is the shape parameter at the end of the wake, V is the freestream velocity, θ_i is the momentum thickness at "downstream infinity," and $\underline{x}$ and $\underline{y}$ are a function of angle of attack (Equations 9 and 10) (Ref. 3):

$$\underline{x} = x * cos \cos(\alpha) + y * si\,n(\alpha) \qquad (9)$$

$$\underline{y} = y * cos \cos(\alpha) + x * si\,n(\alpha) \qquad (10)$$

The number of panels and panel density ratio utilized in XFOIL for this study were 425 and 0.18, respectively.

UNS2D

UNS2D is a mid-fidelity flow solver developed by Sukra-Helitek for generation of 2D aerodynamic coefficients of an airfoil in AFTGen. Rather than utilizing a panel around the surface of the airfoil like XFOIL, UNS2D uses a hybrid of an O-grid near the surface of the airfoil and an unstructured triangular grid farther from the airfoil surface (Ref. 5 and 6). The mathematical model of UNS2D results in a longer run time for the aerodynamic properties within c81 tables to reach convergence at various Mach numbers and angles of attack, elaborated as follows.

UNS2D's approach to obtaining values used for c81 tables utilizes the unsteady-state Navier-Stokes equations in 2D space (Ref. 5 and 6). These equations govern the motion of fluid flow and include the partial derivative terms in the continuity equation and momentum equations. As implied, rather than looking at it in a 3D space, UNS2D utilizes the partial derivatives of pressure, time, and the two directions in the cartesian coordinates generally noted as the x-direction and y-direction.

The grid generation in UNS2D discretizes the domain around the airfoil into a mesh of elements. Serving as a framework to apply the Navier-Stokes equations, the equations are solved at the nodes to calculate the vector field variables such as velocity, pressure, and density (Ref. 5 and 6).

ROTCFD

The Rotorcraft Computational Fluid Dynamics (RotCFD) software, developed by Dr. R Ganesh Rajagopalan, Sukra Helitek, Inc., is a reliable GUI environment to analyze the behavior of the flow around a blade in three-dimensions. Based on the solver interface, the governing equations of the flow are unsteady, incompressible Navier Stokes equations. Regarding the simulation, the first-time step is run with incompressible Navier Stokes equations; the flow can be considered incompressible as the local Mach numbers for the cells fall below 0.25 (Ref. 8). Mach numbers greater than 0.25 are influenced by the velocity of the object, speed of sound in the medium, density of the medium, temperature, and atmospheric conditions (Ref. 8). In these cells, the future time step is calculated using the compressible Navier Stokes equations. These equations incorporate the fundamental principles of mass conservation, momentum conservation, and energy conservation to analyze the fluid motion around the blade. Under the assumption of incompressible flow, several simplifications can be considered regarding the fluid properties. These simplifications involve isothermal temperature, constant volume regardless of the pressure applied, a continuous medium, and Newtonian behavior: constant viscosity across a range of shear rates and maintaining a constant temperature. In this study, the solver considered both compressible and incompressible flow conditions by utilizing the Navier Stokes equation at the local Mach Number for a particular cell. The grid generation panel in RotCFD uses a Cartesian Octree grid to surface geometry and creates the planes along X, Y, and Z.

NACA 0012 and CSUS 001: XFOIL vs UNS2D COMPARISONS

The following section presents a comparison of the results obtained from the flow solvers XFOIL and UNS2D of the NACA 0012 airfoil and the airfoils used in the CSUS 001 rotor blade. Moreover, a common approach was taken before running these solvers, such as setting appropriate inputs to obtain reasonable and precise results with low non-convergence rates. Table 2 conveys the input settings for the flow solvers. The Re/M of 3.24 x 10^6 was chosen because it was the lowest value that could be used while avoiding significant non-convergence. A low Re/M was preferable to match the wind tunnel Re as closely as possible.

Table 2: Flow Conditions and Primary Inputs for XFOIL and UNS2D

α Range	[-20, -15, -10, -8, -6, -4, -2, 0, 2, 4, 6, 8, 10, 15, 20]
M_{Tip} Range	[0.1, 0.2, 0.3]
Re/M	3.24 x 10^6

CSUS 001 consists of three airfoils with thicknesses of 11%, 13%, and 15% (Table 1). The solvers provided the aerodynamic performance c81 tables for each CSUS 001 airfoil and the NACA 0012 airfoil, which consist of section lift coefficients (c_l), section drag coefficients (c_d), and section moment coefficients (c_m) at the corresponding angle of attack (α) and M_{Tip} number, which refers to the speed of the tip of the blade relative to the speed of sound in the ambient air.

NACA 0012

As observed in Figure 2, for the NACA 0012 UNS2D result, the section lift coefficient at both extremes of the angle of attacks tested is slightly below ± 1 while the XFOIL section lift coefficient at ± 10 angle of attack is slightly above ± 1. There is little discrepancy between the UNS2D and XFOIL NACA 0012 section lift coefficient results. Figure 3 illustrates the section drag coefficient of NACA 0012 with the UNS2D result showing a maximum section drag coefficient of 0.0375. For XFOIL the section drag coefficient shows a maximum value of 0.014, less than half of the UNS2D result. The NACA 0012 section moment coefficient observed in Figure 4 shows similar results between UNS2D and XFOIL between an angle of attack of ± 5. Outside of this angle of attack range the UNS2D and XFOIL results diverge.
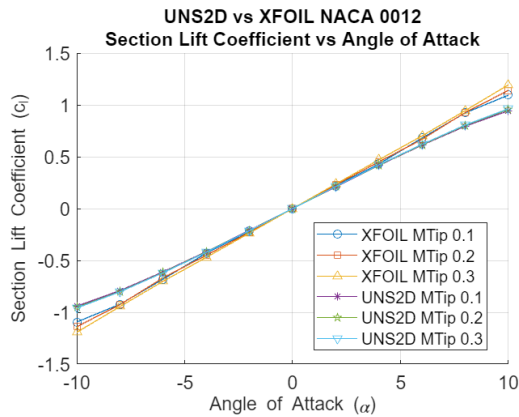
Figure 2: Section Lift Coefficient vs Angle of Attack (NACA 0012 UNS2D and XFOIL)
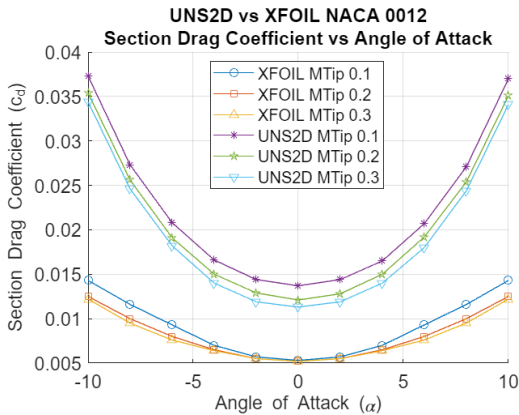
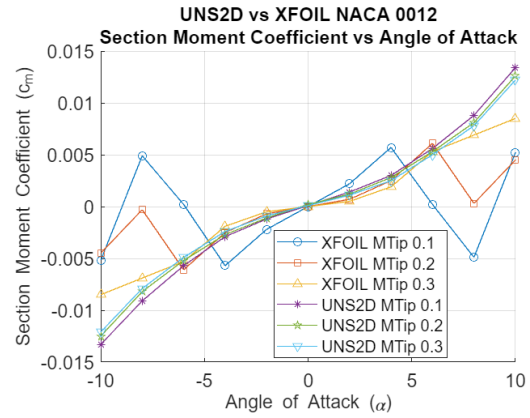**Figure 3: Section Drag Coefficient vs Angle of Attack (NACA 0012 UNS2D and XFOIL)**

Figure 4: Section Moment Coefficient vs Angle of Attack (NACA 0012 UNS2D and XFOIL)

CSUS 001

For the CSUS 001 rotor, each airfoil profile will be assessed to determine the aerodynamic characteristics as the CSUS 001 rotor is composed of all three of these airfoils. The section lift coefficients for the CSUS 001 airfoil produced by UNS2D, Figures 5, 6, and 7, show a positive linear relationship with the angle of attack, except between the angle of attack range of -10 to -6 in which a steady to decreasing section lift coefficient is observed. On the other hand, the XFOIL results do not show the same negative angle of attack behavior observed in the UNS2D results. Instead, the section lift coefficient versus angle of attack result for XFOIL is a quadratic relationship, almost resembling a linear line. However, there is little discrepancy between UNS2D and XFOIL section lift coefficient values, especially for Airfoil 3 for which the results are almost identical.
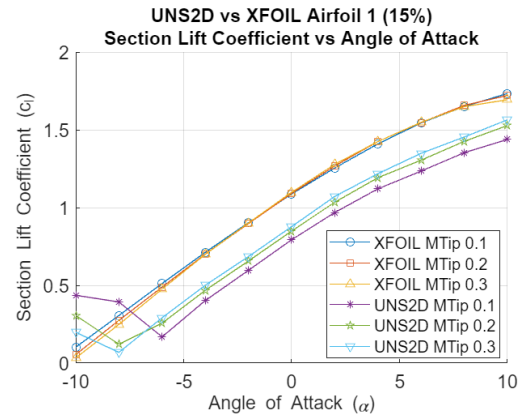

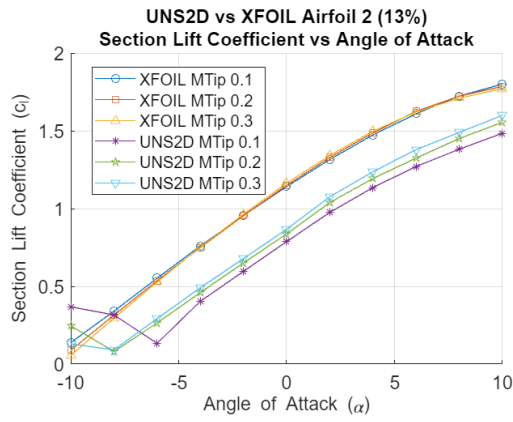**Figure 5: Section Lift Coefficient vs angle of Attack (CSUS 001 Airfoil 1 UNS2D and XFOIL)**

5

Figure 6: Section Lift Coefficient vs Angle of Attack (CSUS 001 Airfoil 2 UNS2D and XFOIL)
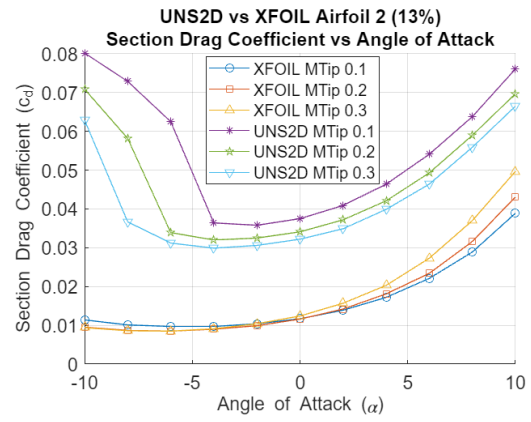

Figure 9: Section Drag Coefficient vs Angle of Attack (CSUS 001 Airfoil 2 UNS2D and XFOIL)
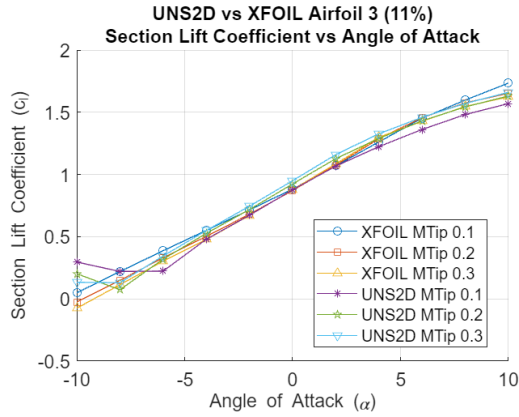

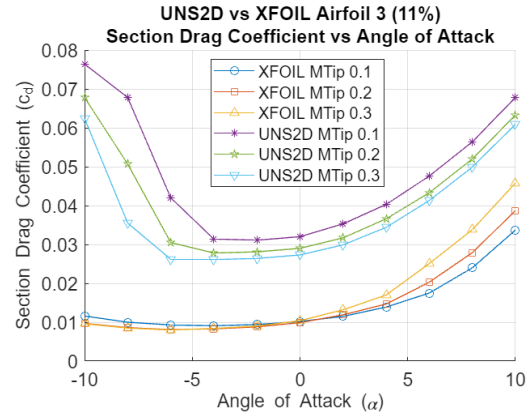**Figure 7: Section Lift Coefficient vs Angle of Attack (CSUS 001 Airfoil 3 UNS2D and XFOIL)**

Figure 10: Section Drag Coefficient vs Angle of Attack (CSUS 001 Airfoil 3 UNS2D and XFOIL)

As seen in Figures 8, 9, and 10, the CSUS 001 UNS2D dataset consists of a pattern where the section drag coefficient is similar to NACA 0012 in the sense that there is a higher section drag coefficient between the angles of attack of -10 to -4 for all three tip Mach numbers. The XFOIL section drag coefficient shows a steady increase from an angle of attack of -10 to 10. Throughout Airfoils 1-3 and the three tip Mach numbers, the XFOIL section drag coefficient is at least half of the UNS2D section drag coefficient result.
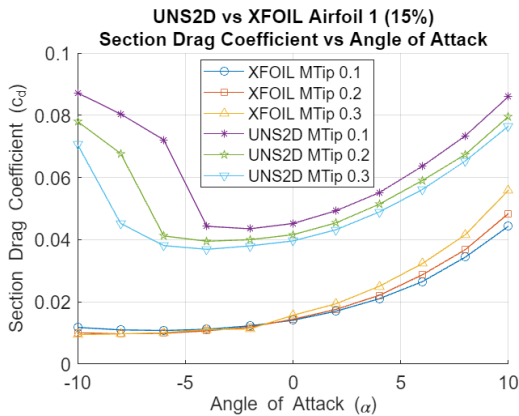
Figures 11, 12, and 13 illustrate the relationship between section moment coefficient and angle of attack for the CSUS 001 airfoils resulting from UNS2D and XFOIL. For Airfoils 1 and 2, the results of both solvers agree at an angle of attack of ten. However, UNS2D predicts higher section moment coefficients at lower angles of attack. All three airfoils show opposite solver trends between -10 and 0 angle of attack with UNS2D predicting a generally negative slope and XFOIL predicting a positive slope. However, for Airfoil 3, the XFOIL section moment coefficient values surpass those predicted by UNS2D at around -4 to -3 angle of attack while the Airfoil 1 and 2 UNS2D section moment coefficients remain higher than the XFOIL predictions at all except the highest angles of attack investigated.
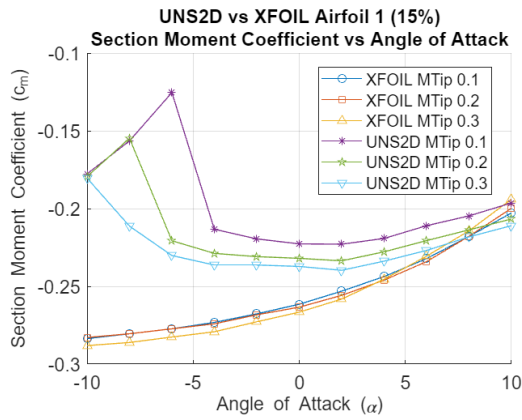

Figure 8: Section Drag Coefficient vs Angle of Attack (CSUS 001 Airfoil 1 UNS2D and XFOIL)

Figure 11: Section Moment Coefficient vs Angle of Attack (CSUS 001 Airfoil 1 UNS2D and XFOIL)
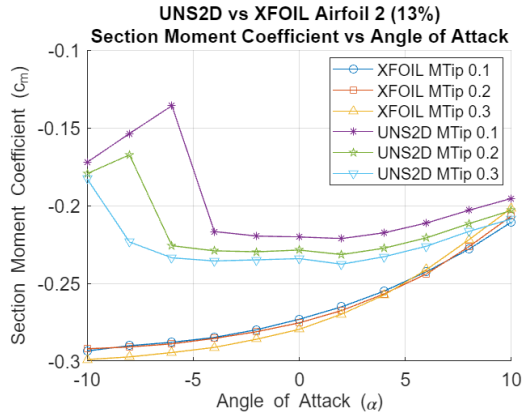

Figure 12: Section Moment Coefficient vs Angle of Attack (CSUS 001 Airfoil 2 UNS2D and XFOIL)
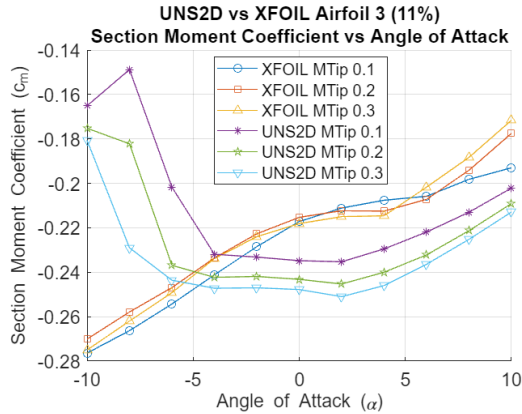

Figure 13: Section Moment Coefficient vs Angle of Attack (CSUS 001 Airfoil 3 UNS2D and XFOIL)

ROTCFD TESTING

APPROACH

RotCFD software was employed for the analysis of rotor performance through computational fluid dynamic simulations. RotCFD provides visual representations of rotor performance under various conditions (Ref. 9). Rotor performance data, such as the coefficient of thrust and total

coefficient of power, can be examined at each collective pitch angle. This visual feedback plays a crucial role in observing the convergence of the solver to a solution. To achieve accurate simulation results, appropriate grid refinement based on the blade geometry, rotor refinement, and setting appropriate time step size is important. These steps involve calculations such as determining the cutout radius of the blade, measuring the distance from the center of rotation to the unnormalized blade tip, and measuring the distance from the center of rotation to each radial station along the blade. The RotCFD inputs utilized are displayed in Table 3.

Table 3: RotCFD Input Settings and Rotor Specifications

Rotor's Refinement	11
Time Steps	3000
Tip Mach Number	0.1, 0.2, 0.3
RPM	2000
Cutout Radius (r/R)	0.389
Radius	0.26543 m
Number of Blades	3
Radial Station Input (r/R) of Airfoil 1 – Thickness 15%	0.445
Radial Station Input (r/R) of Airfoil 3 – Thickness 11%	1.0
Gen. Rotor Refinement	9
Boundary X Cells	5
Boundary Y Cells	5
Boundary Z Cells	5

A common approach in CFD for analyzing rotorcraft flows is to model a rotor as a distribution of momentum sources in the flow. The rotor geometry and the flow behaviors relate to the momentum provided by the rotor. The rotor model calculates rotor performance such as the coefficient of thrust (C_T), total coefficient of power (C_P), and figure of merit (FM). Airfoil tables generated by XFOIL and UNS2D solvers in AFTGen were utilized as the input to determine the rotor performance. The simulations were performed based on NACA 0012 and the CSUS 001 asymmetrical airfoils with various thicknesses: 11%, 13% and 15%, respectively. To comprehensively evaluate the rotor performance across the different hover conditions, a parametric analysis was performed. The simulations involved a range of angles of attack from –10 degrees to +10 degrees. Additionally, the simulations examined a tip Mach number range of 0.1 to 0.3 in 0.1 intervals.

For the Mach 0.1 case, increasing the time step led to better convergence results due to the low speed of flow and incompressibility condition. In some cases, low angles of attack led to convergence issues, and this occurred due to several conditions, such as insignificant pressure differences across the blade as the angle between the rotor blade and

incoming flow is small, characteristics of weak flow, and boundary layers.

A smaller time step was required for the Mach 0.2 and Mach 0.3 cases to obtain sufficient results and improve simulation speed. Based on the RotCFD simulation theory, a Mach number higher than 0.25 is considered an incompressible flow. In essence, the incompressible flow has higher velocity due to escalating external forces, the influence of airfoil geometry, and the behavior of the flow. The decision to set a reasonable time step to obtain convergence results depends on the flow speed, and in other scenarios, the complexity of fluid can affect the convergence results.

RESULTS AND DISCUSSION

The following section represents the results generated by using RotCFD. The relationship between the proportion of ideal power to the real power used in hover, known as the figure of merit (Equation 11), and blade loading (C_T/σ_s), which is the coefficient of thrust of the rotor divided by the relative blade area, known as solidity (Equation 12), are discussed in the following sections. Utilizing the coefficient of thrust and total power coefficient results of NACA 0012 and the asymmetrical airfoil with various thicknesses, the blade's figure of merit can be determined. The calculated solidity (σ_s) value based on the blade area and disk area is 0.228 for both blades.

$$\text{FM} = \frac{\frac{C_T{}^{3/2}}{\sqrt{2}}}{C_P} \qquad (11)$$

$$\sigma_s = \frac{(N_B)(c)}{(\pi R)} \qquad (12)$$

NACA 0012

In this section, the data from RotCFD, which incorporates both XFOIL and UNS2D c81 tables, was analyzed to evaluate the coefficient of power (C_P) and coefficient of thrust (C_T). By analyzing the coefficient of thrust produced with its associated coefficient of power, quantitative assessment of the rotor efficiency for the blade geometry can be performed. Ideally, the blade geometry or solver with a lower coefficient of power associated with a larger coefficient of thrust would be the most efficient. As seen with the RotCFD results from XFOIL and UNS2D in Figure 14, the UNS2D result conveys the highest performance and efficiency at a tip Mach number of 0.3 for producing a coefficient of thrust of 5.7 x 10^{-3} and corresponding coefficient of power of 4.5 x 10^{-4}. Based on the XFOIL result, the highest performance and efficiency is produced at a tip Mach number of 0.3, but the highest coefficient of thrust of 5.7 x 10^{-3} was achieved at a coefficient of power of 3.7 x 10^{-4}. This indicates that XFOIL results demonstrate a slightly better performance and efficiency for the given design space with a C_T over C_P value of 12.7. For transparency, outliers in Figure 14 have not been removed.
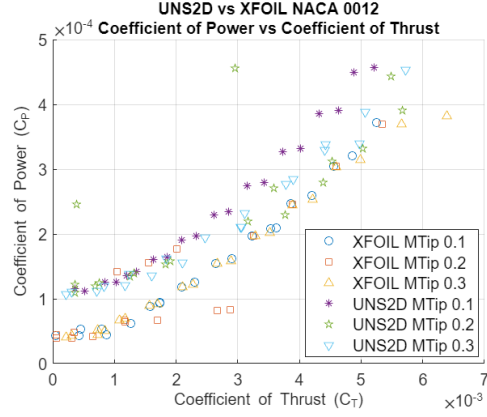

Figure 14: Coefficient of Power vs Coefficient of Thrust (NACA 0012 UNS2D and XFOIL)

In this section, figure of merit, which describes the efficiency of a rotor, is compared against blade loading, which defines how the aerodynamic forces are distributed along the blade, by examining the figure of merit versus (C_T/σ_s) plots based on the results obtained from XFOIL and UNS2D. This analysis indicates that the rotor blade achieves an optimal balance between the generation of lift and efficiency at different tip Mach numbers. Furthermore, it can ensure that the rotor is efficiently generating thrust and functioning optimally by avoiding factors limiting the optimum blade loading.

At $M_{Tip} = 0.1$, Figure 15 shows that the maximum hover figure of merit is about 0.75, which occurs at a blade loading of 0.021 based on XFOIL. On the other hand, the maximum figure of merit is 0.58 at a blade loading of 0.023 for $M_{Tip} = 0.1$ based on UNS2D.

Results from both XFOIL and UNS2D for M_{Tip} values of 0.2 and 0.3 followed a similar pattern as stated above. The optimal blade loading for XFOIL was found to be more efficient compared to UNS2D. Specifically, for $M_{Tip} = 0.2$, the optimal blade loading occurred at a figure of merit of 0.75 for XFOIL, whereas for UNS2D, the highest figure of merit is 0.69. For $M_{Tip} = 0.3$, the optimal blade loading occurred at a figure of merit of 0.81 for XFOIL and 0.73 for UNS2D.

These XFOIL and UNS2D results indicate that the figure of merit is slightly higher at $M_{Tip} = 0.3$ than the other tested tip Mach numbers. This illustrates that the rotor is more efficient at higher speeds. While XFOIL results show more efficiency than UNS2D results, UNS2D data meets the fundamental principle of a rotor's figure of merit not exceeding 0.8.
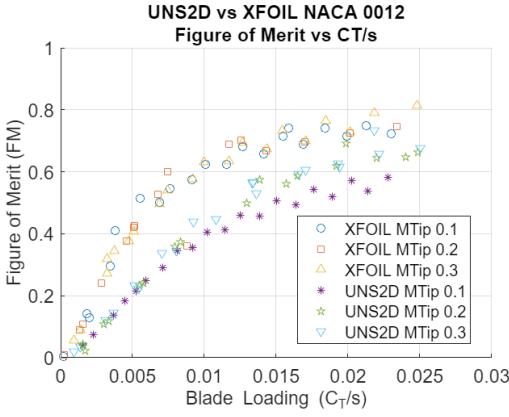
Figure 15: Figure of Merit vs Blade Loading (NACA 0012 UNS2D and XFOIL)

Another measurement of performance of the blade geometry on the rotorcraft hub configuration is the measurement of C_T/σ_s versus the collective (deg.). By looking at the datasets generated by RotCFD from the XFOIL and UNS2D c81 tables, the peak performance across different collective angles can be assessed. As seen from the datasets in Figure 16, the deliverable thrust based on the blade geometry increases as the collective angle increases between the ranges of -10 to 10. Figure 16 shows that XFOIL and UNS2D have a minimum blade loading value of -0.021 at a collective angle of -10 and a maximum blade loading value of 0.024 at a collective angle of 10. Figure 16 also illustrates that, regardless of which solver is used, the lift produced by the blade geometry increases with angle of attack. Since the collective angle range tested was between -10 and 10 for this study, the maximum performance in this design space is at a collective angle of 10.
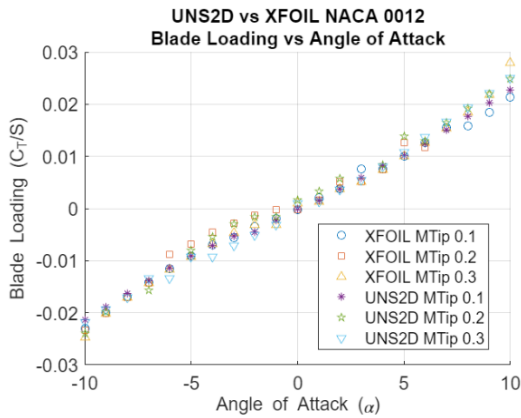

Figure 16: Blade Loading vs Collective (NACA 0012 UNS2D and XFOIL)

CSUS 001

When looking at the coefficient of power versus coefficient of thrust for the custom-designed blade in Figure 17, it is apparent that it differs from the NACA 0012 blade. Furthermore, the values within UNS2D have some datasets between the ranges where the coefficient of thrust is around

zero to 4 x 10^{-3} showing a reverse effect in terms of coefficient of power. This can be attributed to UNS2D's interpretation of the values of coefficient of power, which shows that at some point in the negative angle of attack range, the coefficient of thrust attributed to those values requires a larger coefficient of power. While the initial data points show an increase in efficiency, in the sense that the power needed to deliver a certain thrust force is lower, the efficiency then decreases again where the coefficient of power needed for a larger coefficient of thrust increases more than that of the actual coefficient of thrust value. Both sets of data show that the efficiency and performance of the custom-designed blade are outmatched by the performance of the NACA 0012 blade data. The maximum C_T over C_P value of the CSUS 001 blade was 11.4. Additionally, both data sets and graphs show that the efficiency decreases with a higher angle of attack.
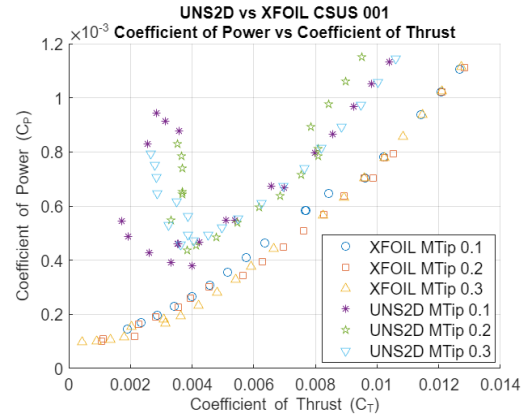

Figure 17: Coefficient of Power vs Coefficient of Thrust (CSUS 001 UNS2D and XFOIL)

The analysis of the figure of merit versus blade loading of CSUS 001 aligns with the optimal blade loading interpretation for NACA 0012. When comparing the data at $M_{Tip} = 0.1$ for XFOIL and UNS2D results, as observed in Figure 18, XFOIL shows a higher hover figure of merit of about 0.95, with a corresponding blade loading of 0.042. On the other hand, UNS2D has a figure of merit of around 0.66 at a blade loading of 0.046.

According to the XFOIL result, the optimal blade loading for $M_{Tip} = 0.2$ occurs at a figure of merit of around 0.984, with a corresponding blade loading of 0.044. Meanwhile, the UNS2D result shows that the optimal blade loading occurs at a figure of merit of 0.66 and a blade loading of 0.036.

At $M_{Tip} = 0.3$, the XFOIL result indicates the decreasing figure of merit pattern after the optimal blade loading point due to stall and profile drag. However, the UNS2D result shows that the data ended at the optimal blade loading point. The optimal blade loading point for the XFOIL can be examined at the figure of merit of 0.943, and the corresponding blade loading point is 0.045. On the other hand, the UNS2D result shows that the optimal blade loading

point corresponds to a figure of merit of 0.675 and blade loading of 0.046.

These analyses based on the optimal blade loading for both XFOIL and UNS2D results indicate that the rotor is more efficient at $M_{Tip} = 0.2$ regarding the XFOIL result, while the UNS2D result shows that the rotor is more efficient at $M_{Tip} = 0.3$. However, based on the fundamental principle of a rotor's figure of merit, the UNS2D result would be more reliable for examining the efficiency of rotor operation. The unrealistically high figure of merit values produced by XFOIL for the CSUS 001 blade indicates that the UNS2D result for both NACA 0012 and CSUS 001 is more accurate to real-world expectations.
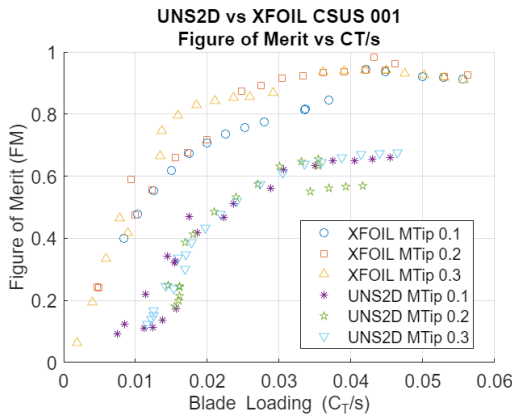

Figure 18: Figure of Merit vs Blade Loading (CSUS 001 UNS2D and XFOIL)

Performance of the CSUS 001 blade is examined in Figure 19 by examining blade loading versus collective. According to the XFOIL and UNS2D generated datasets for CSUS 001, the lift produced by the blade geometry increases as the collective angle increases between the range of –10 to 10.

XFOIL data indicates a minimum blade loading value of 0.0019 at a collective angle of –10 and a maximum blade loading value of 0.056 at a collective angle of 10. On the other hand, UNS2D data shows that a minimum blade loading occurs at 0.0075 and corresponds to a collective angle of –6 and the maximum blade loading value is 0.046 at a collective angle of 10.

The test data generated by both solvers within the examined collective angle range of –10 to 10 degrees indicates that the blade design achieves a balance between thrust generation and efficiency. The optimal point for the CSUS 001 blade was achieved at a collective angle of 10. The XFOIL solver suggests $M_{Tip} = 0.2$ for peak efficiency, while the UNS2D solver points towards $M_{Tip} = 0.3$.
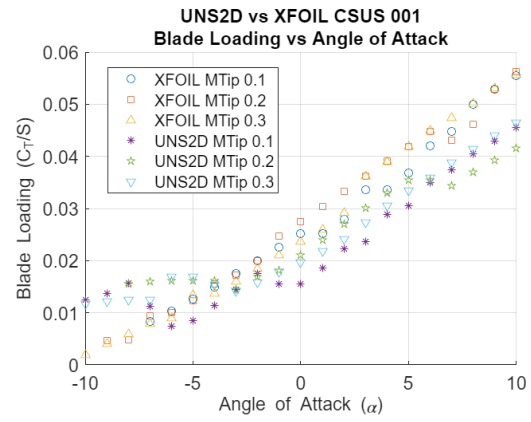

Figure 19: Blade Loading vs Collective (CSUS 001 UNS2D and XFOIL)

EXPERIMENTAL TESTING

To confirm the section lift and drag coefficient values generated in AFTGen by XFOIL and UNS2D were accurate, they were compared to experimental data for the respective airfoils. Using the three airfoils developed in this study and NACA 0012, four test sections were 3D printed with Polylactic Acid (PLA). The testing was done using the California State University (CSU), Sacramento, 2-foot by 2-foot wind tunnel. Figure 20 depicts the wind tunnel experimental setup.
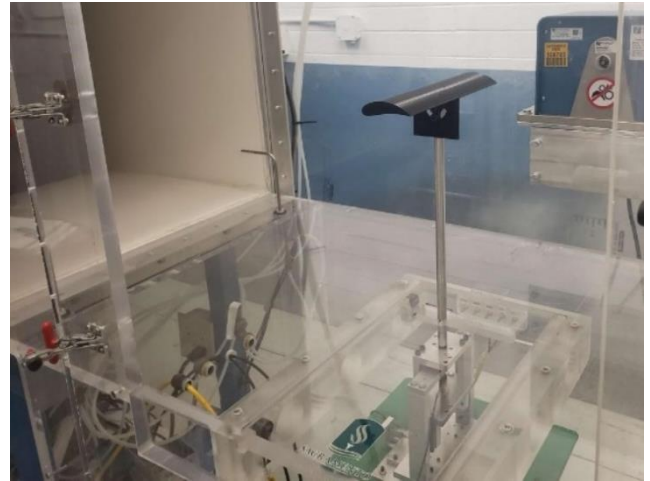

Figure 20: Experimental Wind Tunnel Testing Setup

The experimental data obtained from the wind tunnel was collected with a load cell that effectively measures the lift and drag of an attachment inside the wind tunnel. To ensure that the data gathered was precise, the base values for the lift force and drag force were observed without the 3D printed airfoil attachments, making sure to do this each time the attachment was changed to ensure consistency in subsequent tests. For the experimental tests with the airfoil attachments inside of the wind tunnel testing area, the airfoils printed had an extrusion at the bottom of the airfoil to allow for a pivot screw to be attached and a secondary screw to allow for the angle of

attack to be changed. A digital angle finder was utilized to determine the angle of attack of each airfoil within the wind tunnel, where the data was observed with the angle of attack varying incrementally by 1 degree from -10 to 10 degrees. The final output load values were subtracted from the static loads and converted to section lift and drag coefficients utilizing Equations 13 and 14. These were then compared to the c_l and c_d values from the c81 tables that were created in AFTGen. Section moment coefficient was not experimentally measured.

$$c_l = \frac{(2 * F_l)}{(\rho * v^2 * A)} \tag{13}$$

$$c_d = \frac{(2 * F_D)}{(\rho * v^2 * A)} \tag{14}$$

Additionally, the values for the wind tunnel such as pressure, temperature, humidity, density, dynamic viscosity, and wind speed were measured to allow for the determination of the Reynolds number within the wind tunnel (Table 4 and Equation 15).

Table 4: Wind Tunnel Airflow Data

Pressure	$101000\ Pa$
Temperature	$296.56\ Kelvin$
Humidity	54.2 %
Air Density	$1.18\ kg/m^3$
Dynamic Viscosity	$1.83 * 10^5\ Pa * s$
Freestream Velocity	$34\ m/s$
Reynolds Number	$1.39 * 10^5$

$$Re = \left(\frac{\rho * V * c}{\mu} \right) \tag{15}$$

A freestream velocity of 34 m/s was the highest achievable speed of the wind tunnel. The highest freestream velocity was used to maximize the tested Re. Additionally, utilizing this freestream velocity meant the airfoils were being tested at a Mach number of 0.1 which was ideal for comparison to flow solver results. Given the dimensions of the wind tunnel testing chamber, the maximum achievable Re using a chord of 2ft was 1.34×10^6. However, this Re is still an order of magnitude below the flow solver Re at a Mach number of 0.1. Additionally, a 2ft chord rotor blade was unfeasible to fabricate due to 3D printer build plate dimension limitations.

3D PRINTING

Manufacturing of the extruded airfoil profiles for wind tunnel testing was done using a Sovol SV06 3D printer and Ultimaker Cura slicer. For these prints, universal settings were used and are as follows: the infill was set to 100%, with a print quality of 0.2 mm, print speed was left at the default of 50 mm/s, tree supports were used with raft adhesion method to increase plate contact and prevent the prints from toppling over, z-hop was also activated to prevent the nozzle from colliding with the print during traveling. A finer quality was considered but decided against it because the surface finish

seemed to diminish, as well as the increased time demand for finer quality prints. All other unmentioned parameters were left at the slicer default. All specimens produced generated a smooth finish.

COMPUTATIONAL VS EXPERIMENTAL COMPARISONS

In the interest of comparing computational and experimental data, the airfoil table data generated in AFTGen was compared to the experimental data.

Regarding the section lift coefficient versus the angle of attack for the NACA 0012 airfoil, as seen in Figure 21, the experimental results yield a larger section lift coefficient at angles of attack below 2 degrees and smaller section lift coefficient at angles of attack above 2 degrees compared to the UNS2D and XFOIL computational results. Additionally, as seen in Figure 22, the measured section drag coefficient versus angle of attack in the experimental data is larger at ± 10 degrees compared to the UNS2D and XFOIL computational results.

For Airfoils 1-3 in the CSUS 001 blade design, comparing the section lift coefficient versus angle of attack from UNS2D with the experimental data, as seen in Figures 5, 6, 7, and 21, the experimental results show the same pattern where the section lift coefficient has a stall behavior at around -6 to -10 degrees and increases between the angles of -6 to 10 degrees. It is important to note that this section lift coefficient phenomenon at a low angle of attack was not captured by XFOIL. However, the results of the experimental section lift coefficient are just short of the expected section lift coefficient from the computational data. Similar to the section lift coefficient results, XFOIL was not able to predict the increased section drag coefficient at negative angles of attack, as observed in the UNS2D and experimental results.
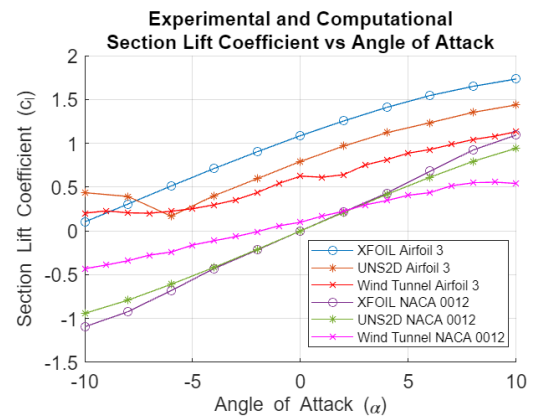

Figure 21: Section Lift Coefficient vs Angle of Attack (UNS2D, XFOIL, and Experimental)
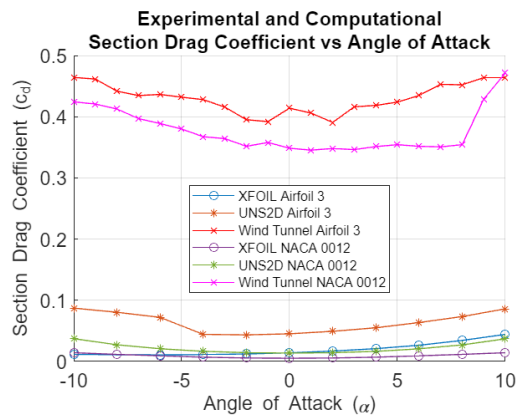
Figure 22: Section Drag Coefficient vs Angle of Attack (UNS2D, XFOIL, and Experimental)

Looking at both the XFOIL and UNS2D interpretation of section drag coefficient versus angle of attack in Figure 22, neither of the NACA 0012 or CSUS 001 datasets have a magnitude similar to the experimental data. This is likely the result of different Reynolds number conditions in the computational and experimental portions of this study. It is important to note that XFOIL and UNS2D were run with a Reynolds number of 3.24×10^7 at a Mach number of 0.1, whereas the experimental runs in the 2ft x 2ft wind tunnel were run with a Reynolds number of 1.39×10^5 at a Mach number of 0.1. As demonstrated experimentally by Dafnis, et al. (Ref. 9), Reynolds number and section drag coefficient are inversely related while Reynolds number and section lift coefficient are directly related. The magnitude of these relationships is also relevant as in increase in Reynolds number significantly decreases section drag coefficient while section lift coefficient only slightly increases. As illustrated in Figures 21 and 22, the same Reynolds number relationships were observed in this study. Therefore, observations on the accuracy of XFOIL and UNS2D could still be made based on the trends of the data despite the significant different in Reynolds number.

CONCLUSION

This study compared the accuracy of the 2D flow solvers XFOIL and UNS2D. It was observed that although XFOIL is more time efficient than UNS2D, XFOIL does not provide accurate results for asymmetrical airfoils at negative angles of attack. Furthermore, the inaccuracy of the XFOIL airfoil tables led to unrealistically high figures of merit in the RotCFD simulations. While XFOIL is an excellent tool for quick airfoil table generation for symmetrical airfoils at any angle of attack and asymmetrical airfoils at positive angles of attack, it cannot confidently be used for asymmetrical airfoils at negative angles of attack.

Author contact:
Gianmarco Sahragard-Monfared
G.Monfared@nasa.gov

REFERENCES

1. Kallstrom, K., "Exploring Airfoil Table Generation using XFOIL and OVERFLOW," Aeromechanics for Advanced Vertical Flight Technical Meeting, Transformative Vertical Flight 2022, San Jose, CA, 2022.

2. "AFTGen Final Report," Sukra Helitek, Inc., 2020.

3. Drela, M., "XFOIL: An Analysis and Design System for Low Reynolds Number Airfoils," Low Reynolds Number Aerodynamics, edited by T. J. Mueller, 1989. DOI: https://doi.org/10.1007/978-3-642-84010-4 1.

4. "OVERFLOW Module for AFTGen Application User Manual," Sukra Helitek, Inc., 2020.

5. "UNStructured 2D Solver Application RotCFD 0.9.15 (Beta) Build 402 K04 Theory," Sukra Helitek, Inc., 2018.

6. "UNS2D Module for AFTGen Application User Manual," Sukra Helitek, Inc., 2021.

7. Thakur, G., and Choudhary, N., "Comparative study of symmetrical Vs asymmetrical Vs semi-symmetrical airfoils," WEENTECH Proceedings in Energy, 09 2020, pp. 193–205. DOI: 10.32438/WPE.0602164.

8. Rajagopalan, R., Baskaran, V., Hollingsworth, A., Lestari, A., Garrick, D. P., Solis, E., and Hagerty, B. P., "RotCFD - A Tool for Aerodynamic Interference of Rotors : Validation and Capabilities," American Helicopter Society Future Vertical Lift Aircraft Design Conference, San Francisco, CA, 2012

9. Ballmann, J., Dafnis, A., Korsch, H. J., Buxel, C., Olivier, H., Braun, C., Baars, A., and Boucke, A., "Experimental Analysis of high Reynolds Number structural Dynamics in ETW," 46th AIAA Aerospace Sciences Meeting and Exhibit, 2008. DOI: 10.2514/6.2008-841.